Bulletin of Multi-scale Estimation of Greenhouse Gas Budgets

National Institute for Environmental Studies, Japan
Japan Agency for Marine-Earth Science and Technology, Japan
Meteorological Research Institute, Japan
Chiba University, Japan

National Institute for Environmental Studies
https://www.nies.go.jp/

National Institute for Environmental Studies

16-2 Onogawa, Tsukuba, Ibaraki, 305-8506, Japan
Phone: +81-(0)29-850-2827 Facsimile: +81-(0)29-851-2854
E-mail: www@nies.go.jp http://www.nies.go.jp/

February, 2022

Secretariat of Information Collection and Preparation,
United Nations Framework Convention on Climate Change

Dear Sir / Madame,

As an observer institution of the UNFCCC, we would like to submit a short report of national-, regional-, and global-scale greenhouse gas budgets for the purpose of supporting the first Global Stocktake.

Sincerely,

Nobuko SAIGUSA, Ph.D.
Director of Earth System Division,
National Institute for Environmental Studies
E-mail: n.saigusa@nies.go.jp

Synopsis

This bulletin provides an overview of the greenhouse gas budgets estimated by the SII-8 project, aiming at making contributions to the first Global Stocktake of the Paris Agreement.

1. Introduction

Reliable quantification of global, regional, national, and local greenhouse gas (GHG) budget is essential to achieve the climate goal of the Paris Agreement. Unlike the Kyoto Protocol (1997), all parties to the Paris Agreement (2015) are obliged to provide national inventories of anthropogenic GHG emissions and their nationally determined contributions. To ensure transparency, the Paris Agreement authorized the Global Stocktake (GST), which is a process for taking stock of implementation with the aim of assessing the world's collective progress towards achieving the purpose of the agreement and its long-term goals, every five years. The first GST, assumed to take place in November 2023, consists of three components: 1) Information Collection and Preparation, 2) Technical Assessment, and 3) Consideration of Outputs.

This summary report aims to demonstrate the outcomes of research activities in Japan with respect to information contributions to the first GST. Funded by the Ministry of the Environment of Japan, the SII-8 strategic research project (Comprehensive Study on Multi-scale Monitoring and Modeling of Greenhouse Gas Budgets) was launched in April 2021. The participating research groups evaluated GHG budgets at multiple scales, by using their resources such as observational platforms, advanced models, and inventories (Fig. 1). Such attempts are undoubtedly required, because the GST should take into consideration inputs on equity and make use of the best available science in a cross-cutting manner. This report gives a brief overview of the methodology adopted in this project and shows key results that are expected to support the first and following GSTs. Advantages of the present study come from 1) integrated deployment of multiple (bottom-up and top-down) approaches, 2) a wide range of spatial scales, and 3) quick reporting to support decision making. In particular, the present study better covered the Asia and Pacific areas, which other regional or global monitoring activities have covered only sparsely.
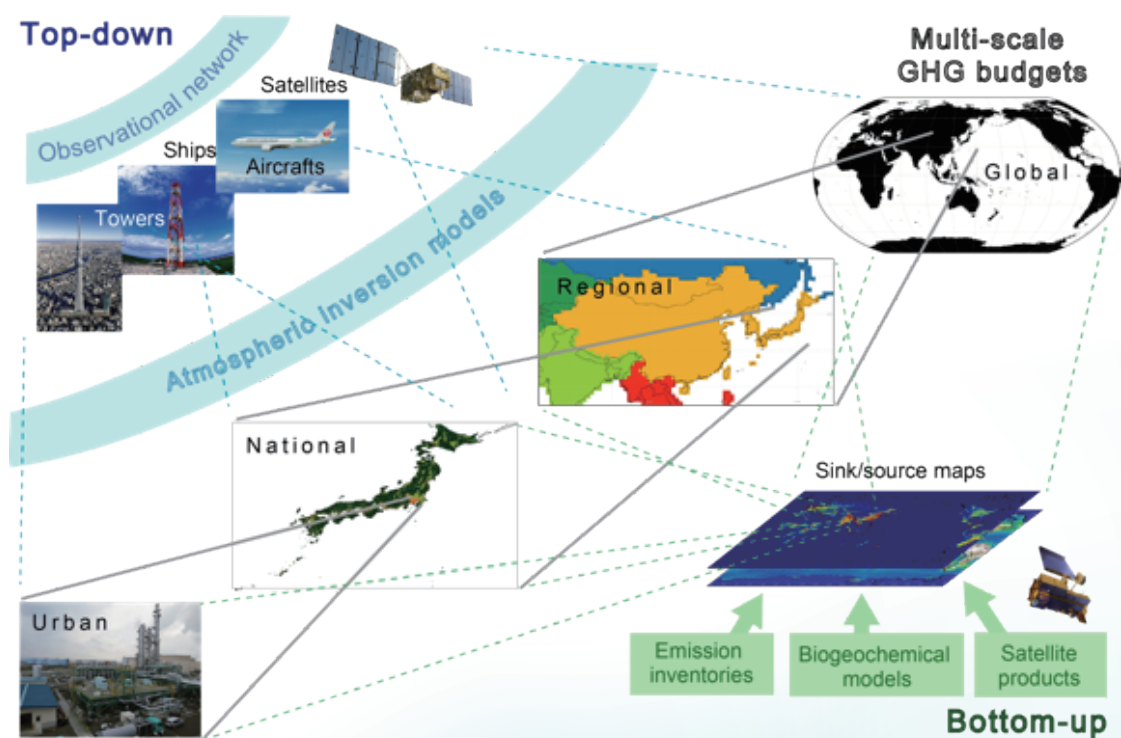
Figure 1. Overview of multi-scale GHG monitoring system using the top-down and bottom-up approaches.

2. Methodology

2.1. Top-down approach

a) Atmospheric observations

Ground observatory, ship, CONTRAIL (aircraft), GOSAT series (satellite) etc.

The Japan Meteorological Agency (JMA), the Meteorological Research Institute, and the National Institute for Environmental Studies (NIES) have been monitoring atmospheric GHGs from a variety of platforms, including ground sites (Mukai *et al.*, 2001; Tohjima *et al.*, 2002; Watanabe *et al.*, 2000; Tsutsumi *et al.*, 2006), JMA research vessels (Ishii *et al.*, 2011; Ono *et al*, 2019), commercial cargo ships (Terao *et al.*, 2011; Tohjima *et al.*, 2012), aircrafts (Matsueda *et al.*, 2002; Machida *et al.*, 2008; Tsuboi *et al.*, 2013; Umezawa *et al.*, 2020), and satellites (Yokota *et al.*, 2009; Yoshida *et al.*, 2013). The GHGs are measured on-site or in air samples that are collected in canisters and sent back to the individual laboratories to determine mole fractions of the GHGs and C/H/N isotopic composition. The mole fractions of the GHGs, including CO_2, CH_4, and N_2O, are precisely determined based on highly compatible standard scales (Tsuboi *et al.*, 2017). The time courses of CO_2 over the Asia Pacific area from 2010 through 2021 are plotted in Fig. 2, showing the spatio-temporal variability of CO_2 at background (e.g., MNM), continental (e.g., NTL), and urban (e.g., YYG) sites. These observed data are provided immediately to the atmospheric inversion systems, following strict quality assurance and quality control procedures.
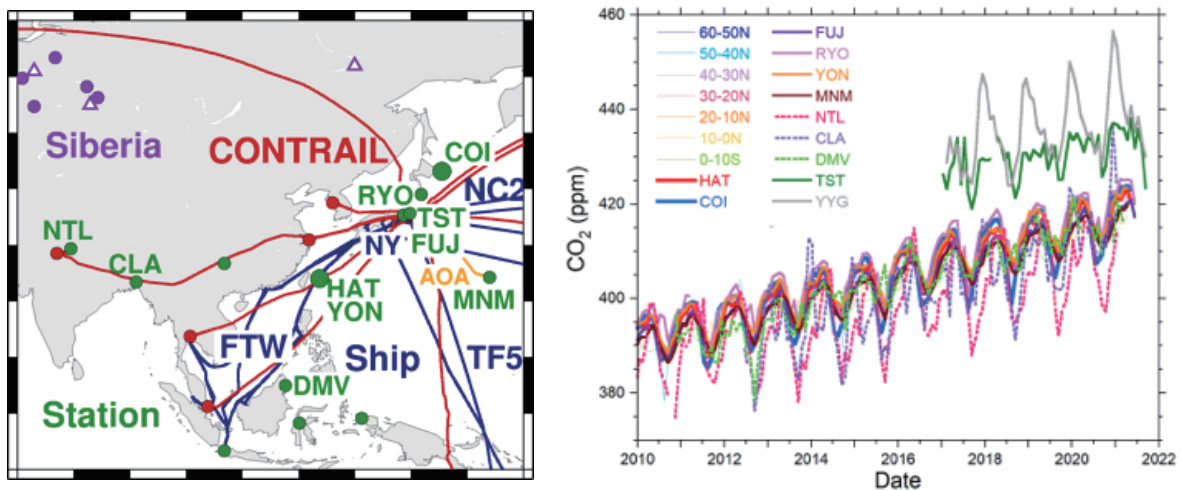
Figure 2. (left) Map showing the locations of the atmospheric GHG observations in the Asia-Pacific region. Green circles represent ground sites, blue lines shipboard routes, and red lines airplane routes. (right) Time courses of atmospheric CO_2 observed over the Asia Pacific region from 2010 through 2021 are shown at monthly intervals.

NIES has observed the atmosphere in Tokyo megacity since 2016. The time courses of atmospheric CO_2 observed at Tokyo Skytree (TST) are plotted in Fig. 3, showing large (up to 100 ppm) increases in CO_2 from baseline concentrations, which is calculated by smoothly connecting the data below 10th percentile for a 5-day time window. The high-resolution NICAM model indicated that the fossil fuel CO_2 emitted from the Greater Tokyo area was the major source (61% of annual average) of CO_2 increases larger than 20 ppm, supplemented by fossil fuel CO_2 emitted from other areas (15%) and from the biosphere (23%). These observed data and high-resolution modeling are especially useful for monitoring GHG emissions in Tokyo megacity.
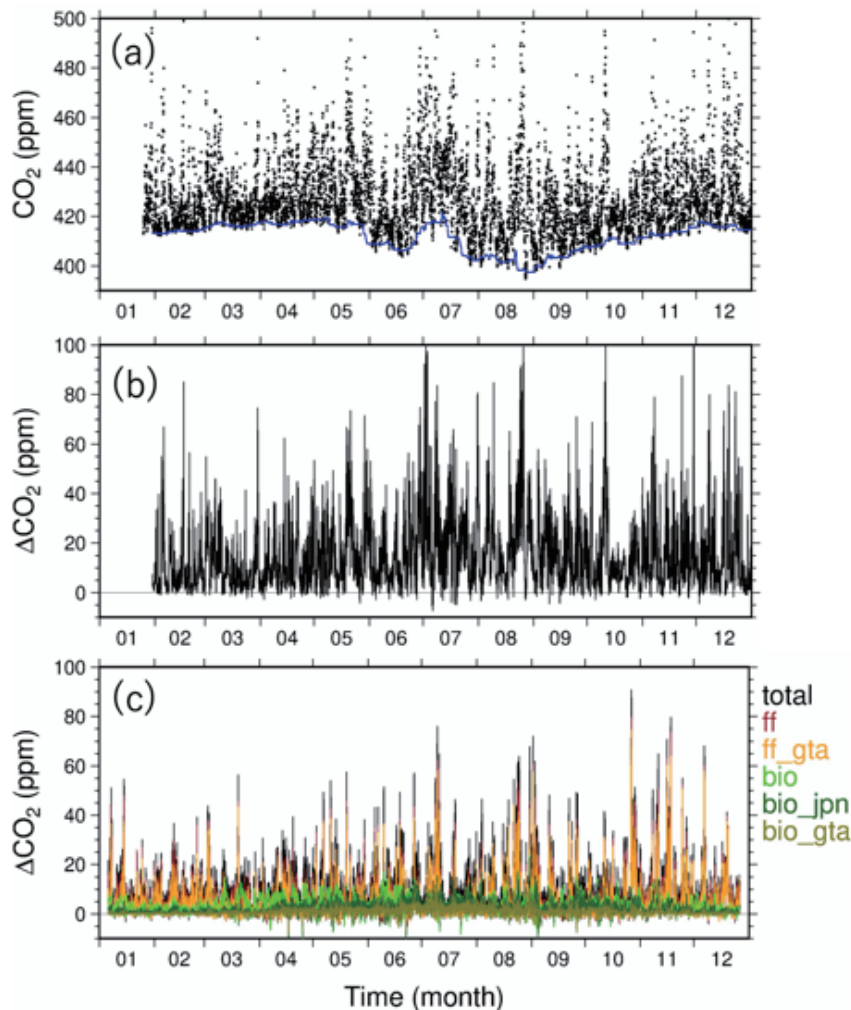
Figure 3. Time courses of (a) the 1-h averaged CO_2 and (b) enhanced CO_2 (ΔCO_2) observed at TST in 2017 from the baseline concentrations, and (c) enhanced CO_2 simulated using the high resolution NICAM model.

b) Atmospheric inversion modeling

NICAM-TM and NISMON:

The Nonhydrostatic Icosahedral Atmospheric Model (NICAM) is a numerical simulation model developed for global high-resolution simulations by the University of Tokyo, JAMSTEC, RIKEN and other Japanese institutes (Satoh *et al.*, 2014). The NICAM-based Transport Model (NICAM-TM) and NICAM-based Inverse Simulation for Monitoring greenhouse gases (NISMON) are used to simulate concentration variations in the atmosphere and estimate surface fluxes of CO_2 and CH_4 (Niwa *et al.*, 2017a,b). NICAM-TM has been developed for GHG studies from the study of Niwa *et al.* (2011). In NISMON, the four-dimensional variational method, which is a state-of-the-art data assimilation/inversion method, is implemented to exploit a large number of observations and estimate high-resolution (model grid point) flux values (i.e., large dimensional problems) (Niwa *et al.*, 2017a,b). Its application to estimate CO_2 fluxes (NISMON-CO_2) was demonstrated by Niwa *et al.* (2021). Its long-term analysis (Niwa, 2020) was conducted using version 2021.1 (NISMON-CO_2 v2021.1; Niwa, 2020) and used in the synthesis analysis of the global carbon cycle by Global Carbon Project (Friedlingstein *et al.*, 2020, 2021). The prior fluxes of NISMON-CO_2 v2021.1 are composed of the fossil fuel emissions of GCP-GridFED (Jones *et al.*, 2021); terrestrial biosphere fluxes of a process-based terrestrial ecosystem model, the Vegetation Integrative SImulator for Trace gases (VISIT; Inatomi *et al.*, 2010, Ito and Inatomi, 2012, Ito, 2019); the satellite-based biomass burning emissions product, Global Fire Emissions Database (GFED) v4.1s (van der Werf *et al.*, 2017); and shipboard measurement-based ocean flux data of the Japan Meteorological Agency (Iida *et al.*, 2021).

MIROC4-ACTM:

The Model for Interdisciplinary Research on Climate, version 4 (MIROC4) is an earth system model developed at JAMSTEC, in collaboration with the University of Tokyo and NIES (see Box). MIROC4-ACTM is the atmospheric chemistry transport version of MIROC4 (Patra *et al.*, 2018). Simulations of long-lived gases in the atmosphere (CO_2, CH_4, N_2O, SF_6) are performed at a horizontal resolution of T42 spectral truncations (~2.8° × 2.8° latitude-longitude grid) with 67 vertical hybrid-pressure layers between the Earth's surface and 0.0128 hPa (~80 km). The simulated horizontal winds (U, V) and temperature (T) are nudged with the Japan Meteorological Agency Reanalysis data product (JRA-55; Kobayashi *et al.*, 2015) over the altitude range of ~980 to 0.018 hPa for better representation of the atmospheric transport at synoptic and seasonal timescales. We tested the large-scale interhemispheric transport and Brewer-Dobson circulation in the MIROC4-ACTM using SF6 simulations in the troposphere and CO_2-derived age of air in the troposphere and stratosphere (Bisht *et al.*, 2021; Patra *et al.*, 2018; and references therein). The MIROC4-ACTM inversion system optimizes monthly-mean fluxes from 84 regions of the globe for CO_2 and N_2O (Saeki and Patra, 2017; Patra et al., 2022) and 54 land regions for CH_4 (updated from Chandra *et al.*, 2021a).
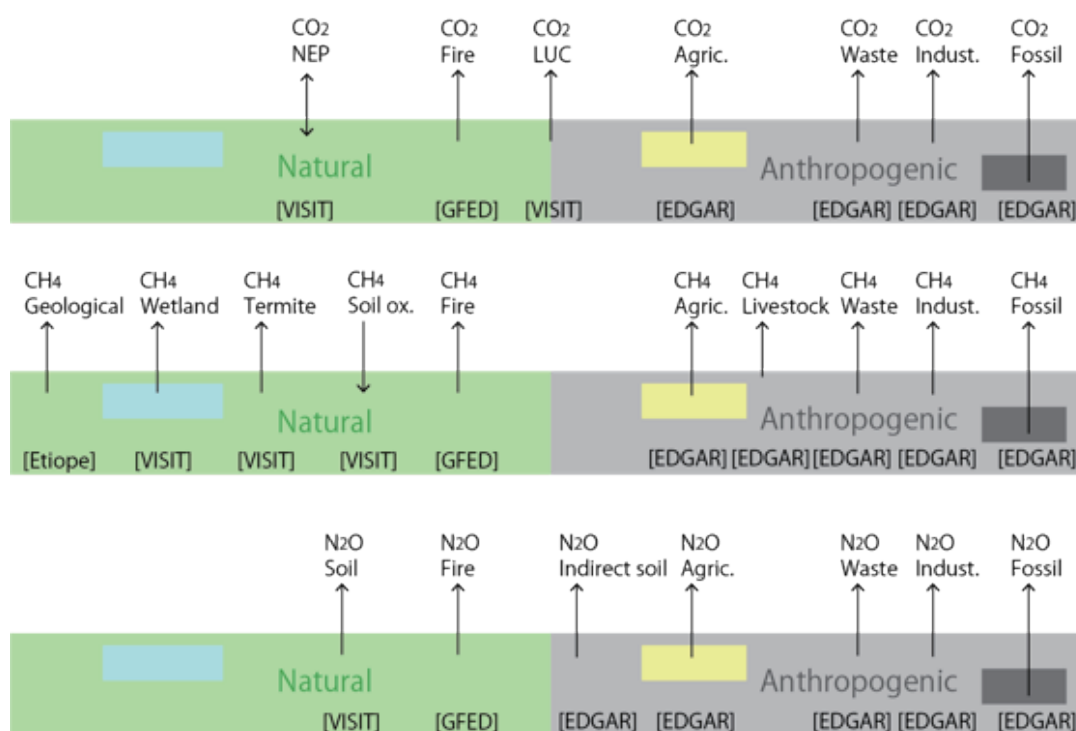
Figure 4. Summary of the bottom-up estimation of GHGs budgets: CO_2 (upper), CH_4 (middle), and N_2O (bottom). Method and data used for each flow are shown in [brackets]. VISIT: Vegetation Integrative SImulatr for Trace gases, GFED: Global Fire Emission Database.

2.2. Bottom-up approach

The bottom-up approach estimates surface GHG sinks and sources by using emission inventories, biogeochemical models, and surface remote sensing (Fig. 4), and therefore is independent from atmospheric observational data. The bottom-up approach has advantages in spatial resolution and sectorial explicitness, but disadvantages in time-lag and data-specific uncertainties. In general, the bottom-up approach uses multiple data sources to cover a variety of sinks and sources for both natural and anthropogenic sectors. In this project, we mainly used a biogeochemical model to estimate GHG sources and sinks of natural sectors and an emission inventory for anthropogenic emissions. Because simulation of wildfire is highly uncertain in the biogeochemical model, a satellite-derived product was used.

a) Biogeochemical model

The process-based terrestrial ecosystem model VISIT was used to simulate GHG exchange of natural ecosystems. The model has been used in regional and global studies of terrestrial GHG budgets and examined with atmospheric and field measurement data (e.g., Patra *et al.*, 2011, 2022; Chandra *et al.*, 2021a). The model simulates biogeochemical processes of natural and agricultural ecosystems; their area fraction-weighted values represent the total flux at each grid point. The model consists of biogeophysical (e.g., radiation budget) and biogeochemical schemes and simulates water, carbon, and nitrogen cycles. In the fraction of cropland, agricultural practices such as planting, harvesting, and fertilizer input are considered in a simplified manner (Ito *et al.*, 2018).

Box. Earth System Model

To quantitatively assess how much the efforts of countries to reduce GHG emissions will lead to global warming mitigation, we use global warming projections by Earth system models (ESMs). By giving anthropogenic CO_2 and other anthropogenic emission scenarios, ESMs can project future CO_2 sinks by land and ocean, changes in CO_2 concentrations, and subsequent climate change, together with impacts from other non-CO_2 GHG species. This is a collaborative study with the TOUGOU (Integrated Research Program for Advanced Climate Models), funded by the Ministry of Education, Culture, Sports, Science and Technology, Japan. Figure Box-1 shows historical simulation of global temperature change by an Earth system model and a climate model emulator; by averaging multiple ensemble simulations with slightly different initial conditions, it is possible to extract signals of global temperature rise from projections of global emission reduction. We plan to assess the effectiveness of emission reductions, based on the latest anthropogenic emission data and ESM simulations.
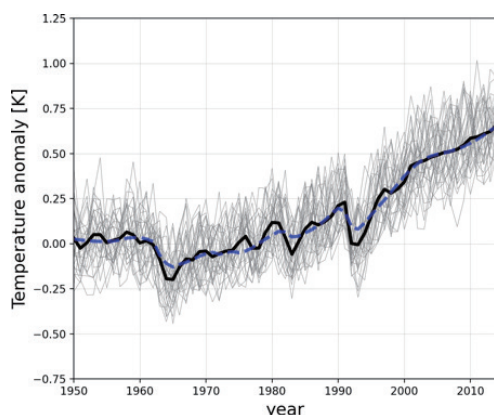
Figure Box-1. Near-surface air temperature change (represented as the difference from the 1961–1990 average) simulated by an Earth system model, MIROC-ES2L (Hajima et al., 2020). Multiple simulations with different initial conditions (thin lines) were performed for the period of 1850–2014, and the ensemble average is represented by thick black line; the averaged air temperature is well reproduced by a simple climate model (FAIR, Smith et al., 2018) In this case, the simulations were performed with a prescribed CO_2 concentration configuration. The simulated results are available via the Earth System Grid Federation (https://esgf-node.llnl.gov/search/cmip6/, and used extensively in IPCC 6th Assessment Report.

---

b) Emission inventory and satellite products

Anthropogenic emission database

Anthropogenic emission inventories were used for the bottom-up estimation, as well as prior data of atmospheric inversions. The Emission Database for Global Atmospheric Research (EDGAR; Crippa et al., 2020) version 6.0 was used because this dataset covers all GHGs and has high spatial resolution ($0.1°$ × $0.1°$) and explicit sectorial classification. The emission sectors were aggregated into four to five categories: fossil fuel mining, urban and industry, waste including landfill, agriculture, and indirect emission (N_2O from deposition) or livestock (CH_4 only). For comparison, several other emission datasets were referred to: Open-Data Inventory for Anthropogenic Carbon dioxide (ODIAC), Gridded fossil CO_2 emission database (GridFED), FAOSTAT for agricultural emissions, GAINS/IIASA for CH4 and N_2O, and Community Emissions Data System (CEDS).

Fire emission database

Biomass burning emissions of CO_2, CH_4, and N_2O were derived from GFED v4s (van der Werf et al., 2017) including small fires. Emission factors, i.e., emissions per unit weight of biomass burning, were derived from Akagi *et al.* (2011). Because of uncertainties in burnt-area detection algorithms and emission factors, the GFEDv4s-based biomass burning emissions should be examined by comparing them with other similar products such as GFAS (Global Fire Assimilation System) and FINN (Fire Inventory from NCAR).

3. Greenhouse gas budgets

3.1. Top-down approach

Global, regional, and national budgets

Figure 5 shows the global trends in global CO_2 fluxes estimated by two inversion systems (MIROC4-ACTM and NISMON). NISMON inversion used one set of prior flux and model input parameters, but MIROC4-ACTM performed an ensemble of 16 inversions for two sets of prior fluxes and by varying prior flux uncertainty (PFU) and measurement data uncertainty (MDU). The MIROC4-ACTM uncertainties in the predicted fluxes due to different priors are found to be 0.35 and 0.1 Pg C yr^{-1} for global land and ocean, respectively. Ensemble mean land and ocean fluxes are in good agreement with the IPCC 6th Assessment Report "mean" estimates of −2.6 ± 1.14 and −1.7 ± 0.6 (Chandra *et al.*, 2021b). Global total sinks estimated with both NISMON and MIROC4-ACTM are in good agreement with the observed global mean CO_2 growth rate (Fig. 5d), although differences remain in land-ocean partitioning of carbon uptakes in the post-2012 period (Fig. 5b,c).
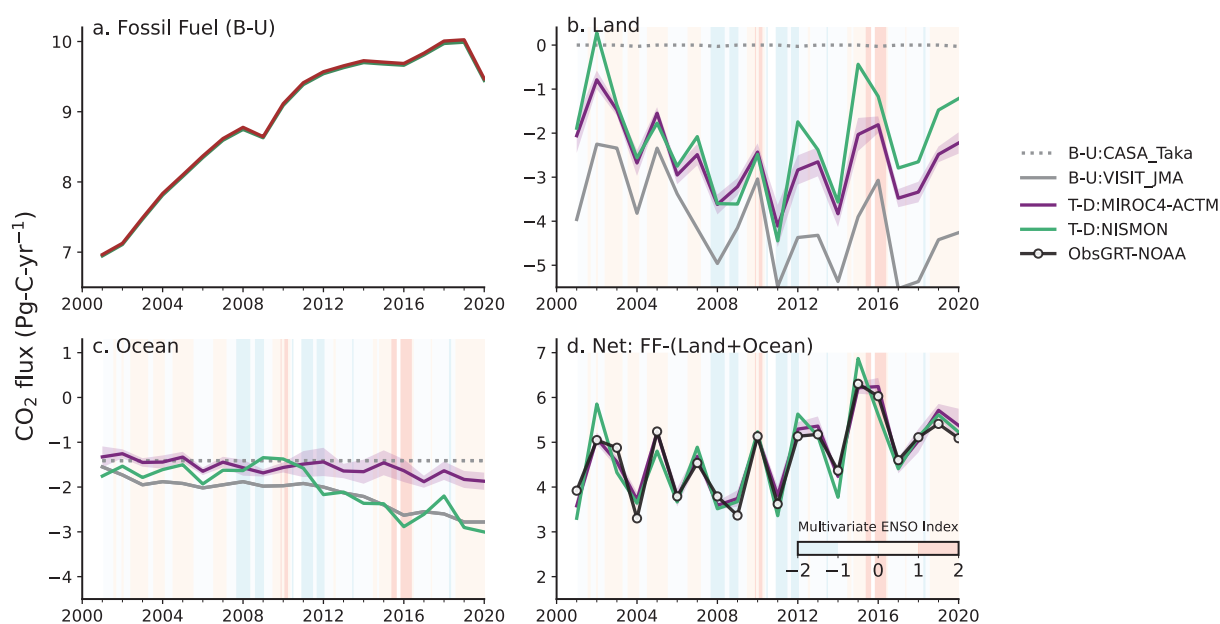
Figure 5. Global annual CO_2 emissions from fossil-fuel (a) and estimated land (b) and oceanic (c) carbon sink from MIROC4-ACTM and NISMON inversions. In panel d, net CO_2 flux (FF emission − land sink − oceanic sink) is compared with the observed global growth rate from the NOAA/ESRL (Dlugokencky and Tans, 2021). CO_2 growth rate is the converted to net flux calculated using a factor 2.13 Pg C ppm^{-1} (d). The background shading in panels b, c and d shows Multivariate El Niño Southern Oscillation (ENSO) Index (Wolter and Timlin, 2011).

Figure 6 shows regional CO_2 fluxes and flux uncertainties from the 16-member ensemble inversions for 15 land regions at 5-yearr intervals for the past two decades, as estimated by MIROC4-ACTM. Flux estimates for all the land regions remain quite uncertain, as seen from the 95th percentiles of the 16-inversion ensemble (error bars) at about 0.3 Pg yr^{-1}. However, by employing the 16-inversion ensemble approach we could obtain flux uncertainties that are an order of magnitude smaller compared to the traditional methods, and often less than the regional fluxes themselves. The mean/median fluxes are consistent for the ensemble inversions and represent the true state of CO_2 flux estimation for the MIROC-ACTM and 50 sites used in the inversion. The changes in regional CO_2 fluxes between 5-year periods are generally attributed to the changes in human induced land use, naturally occurring drought, or fire emission intensities at decadal time scales (Chandra *et al.*, 2021b). The step increases in East Asian CO_2 flux between 2001–2005 and 2011–2015 is suggested to be related to the biased fossil-fuel emissions from China, affecting the natural/managed land flux estimation by inversion (Saeki and Patra, 2017).
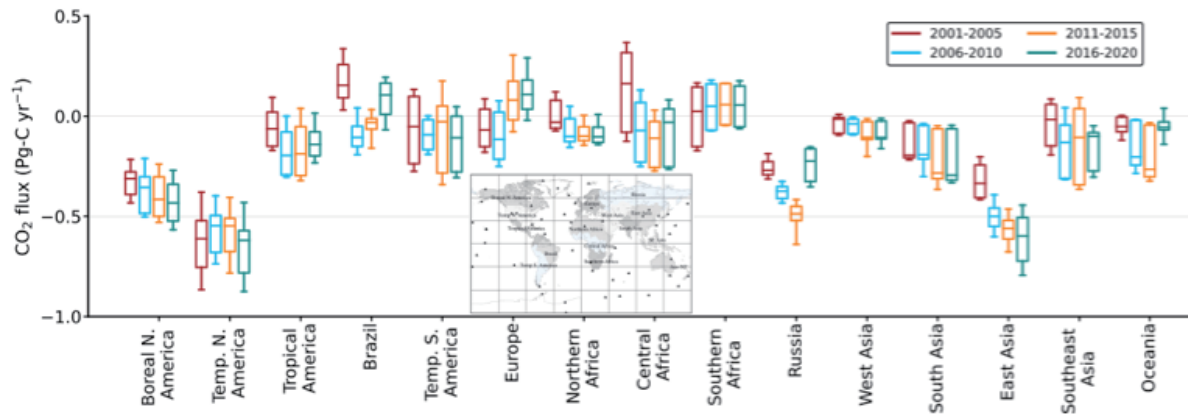
Figure 6. Regional CO_2 fluxes for land using 16 sets of inversion cases for 15 land regions from the MIROC4-ACTM (Chandra et al., 2021b). Box plots each region represent fluxes for 4 different time periods. All 16 inversion cases for each region, based on a different prior, PFU, and MDU, is first averaged for each selected time period. The boxes show 25th and 75th percentiles, and the whiskers show 5th and 95th percentiles from the mean CO_2 flux of 16 ensemble inversion cases. Horizontal lines inside box plots denote the median CO_2 flux of the 16 inversion ensembles. Plot adapted from Chandra et al. (2021b).

Figure 7 shows the CH_4 emission anomalies in the 15 land regions for the period 2001–2020. We take advantage of a joint analysis of region-specific bottom-up emissions for a few dominant sources and regional total top-down emissions to assess the causes of the CH_4 growth rate variabilities during the decrease (1990-1998), quasi-stationary (1999-2005), and regrowth (post-2006) phases. In general, the top-down emission trends agree well with bottom-up emission trends, except for a prominent mismatch for the East Asian region after 2002, suggesting that inventory emissions are in overall agreement with the observed CH_4 concentrations for the control chemical loss case (no interannual variability in hydroxyl (OH) concentration). The agreement between bottom-up and top-down estimates seen here should not be interpreted as a drawback of the inversion but rather an improvement in the a priori emissions, and the bottom-up and top-down emission estimates provide complementary information for better policymaking.
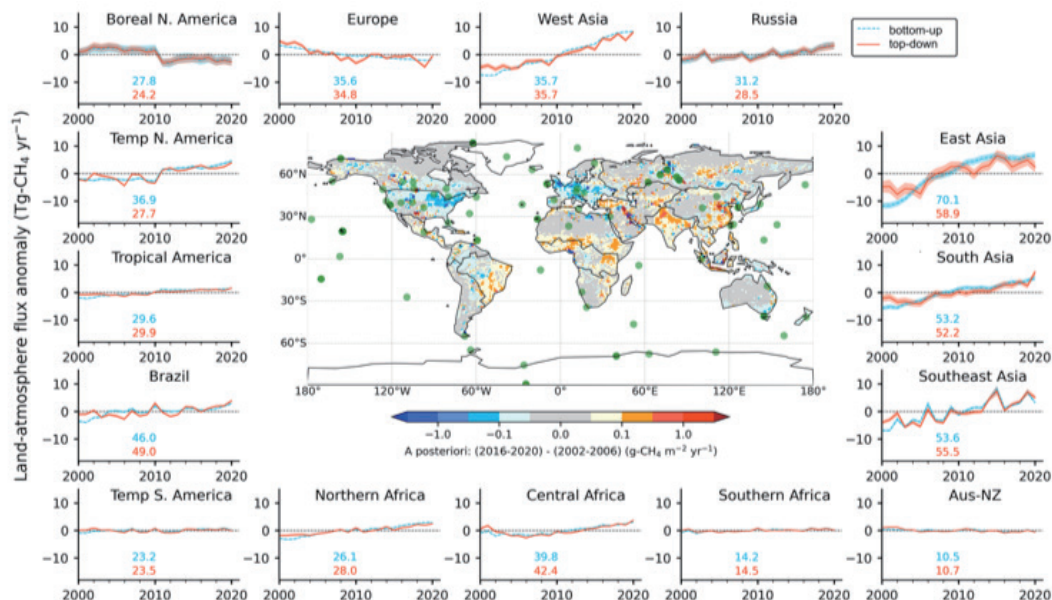
Figure 7. Time series (2003–2020) of regional CH_4 emission anomalies as estimated by 2 cases of MIROC4-ACTM inversions (lines: mean, shade: spread of the 2 cases). Divisions between the 15 regions (black lines) and 60 sites (green circles) are shown on the map of change in emissions between 2016-2020 and 2002-2006. A long-term (2003–2020) mean of individual inversion cases for each region is subtracted to calculate the respective emission anomalies (long-term mean numbers in each panel, in Tg yr⁻¹). Plot adapted from Chandra et al. (2021a) and updated by Dmitry Belikov, Chiba University, by extending the period of inversion until 2020.

Many of the land regions show large interannual variability and systematic increases in predicted N_2O emissions during 1997–2019 (Fig. 8 colored lines), and the systematic increases are in phase with the prior emission scenarios for most regions (grey lines). This suggests that the VISIT model, driven by the fertilizer input data from FAOSTAT, well simulates the N_2O emissions from agricultural activities. The notable exceptions are the Tropical America and Central Africa regions, where the rates of predicted emission increase are at least twice the prior emission increase rate (Fig. 8d, h). Our results confirm a reduction in N_2O emissions from Europe over the period of this analysis. This emission reduction is caused by adaptation of modern technology in the chemical industry, which manufactures nitric acid for fertilizer production mainly and adipic acid for nylon production (ref. EDGAR). Similar reductions in N_2O emissions from Japan are also reported in inventory estimates.
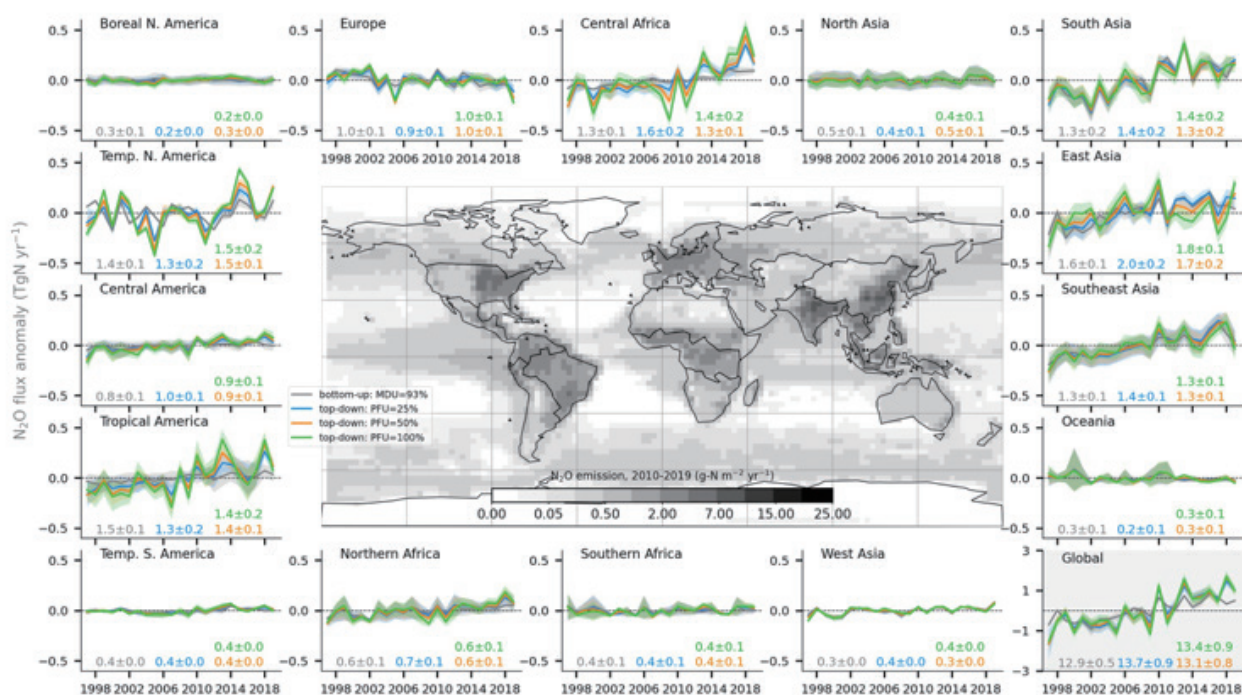
Figure 8. Regional N_2O emissions for the 15-land regions, marked by the dark lines on the 2010s mean emission map, for 3 cases of bottom-up emissions (grey) and top-down emissions by varying prior flux uncertainty (PFU cases: 25%, blue; 50%, orange; and 100%, green). All top-down results correspond to a case of MDU=93% (details in Patra *et al*., 2022). The long-term (1997–2019) mean regional emission (numbers within each panel) are subtracted from the annual mean emission and 1-sigma standard deviation (shaded area) are calculated from different a priori cases. The map in the center shows gridded N_2O emissions. Plot taken from Patra *et al*. (2022).

CO_2 emission changes during and after COVID-19 lockdown in China

In the early phase of the outbreak of the new coronavirus (COVID-19) (January to March 2020), the government of China imposed severe restrictions on socio-economic activity (i.e., a lockdown), which led to a significant reduction in fossil-fuel-derived CO_2 (FF) emissions and other anthropogenic air pollutants. Previous studies revealed that the ratio of the synoptic-scale variations of CO_2 and CH_4 ($\Delta CO_2/\Delta CH_4$ ratio) observed at Hateruma Island (HAT) during winter was a good indicator of the change of the relative emission strengths (Tohjima *et al*., 2014). Careful investigation of the long-term, high-frequency measurements at HAT revealed that the monthly $\Delta CO_2/\Delta CH_4$ ratio markedly decreased in February 2020 (Tohjima *et al*., 2020), while the ratio returned to the level of the preceding 9-year average in January to March 2021 (Fig. 9). Assuming that the CH_4 emissions from China did not vary significantly, our results indicate that the FF emissions from China had rebounded to the pre-COVID-19 level by early 2021.
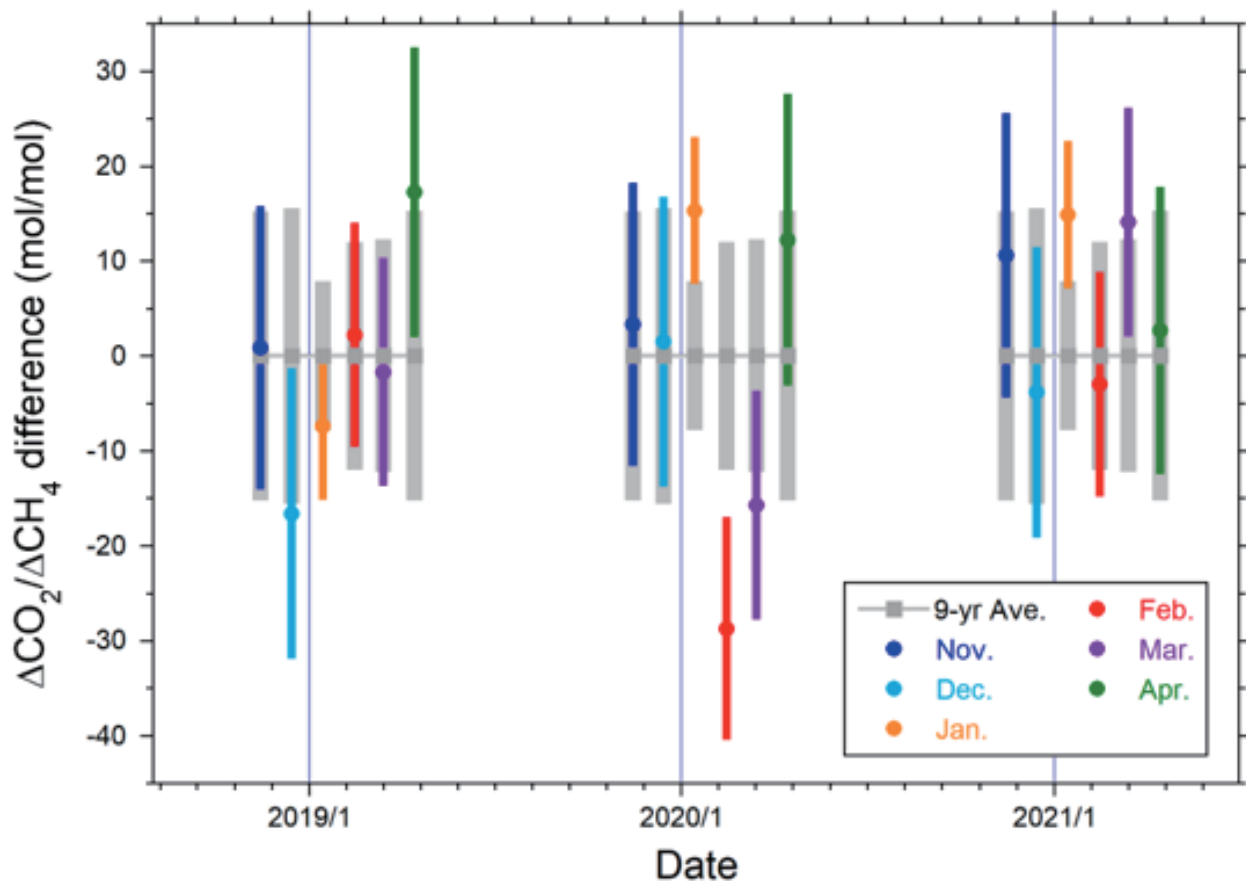
Figure 9. Temporal variations of the difference of monthly $\Delta CO_2/\Delta CH_4$ ratios observed at Hateruma Island from November through April during the three years beginning in November 2018, 2019 and 2020 from the 9-year average. Colored circles and bars represent the average differences and standard deviations for the individual months; grey squares and vertical bars, the average (set at 0) and standard deviations for the same months during the preceding 9 years.

3.2. Bottom-up approach

The bottom-up approach provides global maps of sources and sinks for each GHG and sector (Fig. 4). By aggregating the maps, global, regional, and national GHG budgets were obtained. Note that this procedure allows us to obtain consistent budgets across scales; i.e., the sums of regional and country-based budgets equal the global budget.

Global GHG budget

Annual global natural and anthropogenic CO_2 budgets over 2010 to 2018 were estimated as $-13,900 \pm 2700$ (net sink) and $38,900 \pm 1100$ Tg CO_2 yr^{-1} (source), respectively (mean $\pm$ standard deviation; Fig. 10). In the global total CO_2 budget, land areas were a net source of $25,000 \pm 2500$ Tg CO_2 yr^{-1}. We attribute the net sink by the natural sector mainly to the atmospheric CO_2 fertilization effect and climate change. Most of the terrestrial anthropogenic emissions (96.2%) were associated with industrial and urban activities. Global natural and anthropogenic CH_4 emissions, mainly from land, over 2010 to 2018 were estimated as 166.0 ± 3.4 and 334.0 ± 8.7 Tg CH_4 yr^{-1}, respectively. Using the Global Warming Potential (GWP) over 100 years (34 for CH_4), the annual mean CH_4 source was equivalent to $16,997 \pm 331$ Tg CO_2-eq yr^{-1}. Annual global natural and anthropogenic N_2O emissions in this period were estimated as 10.1 ± 0.3 and 6.4 ± 0.2 Tg N_2O yr^{-1}, respectively. Using the GWP over 100 years (298 for N_2O), the annual mean N_2O source was equivalent to 5501 ± 110 Tg CO_2-eq yr^{-1}.

9
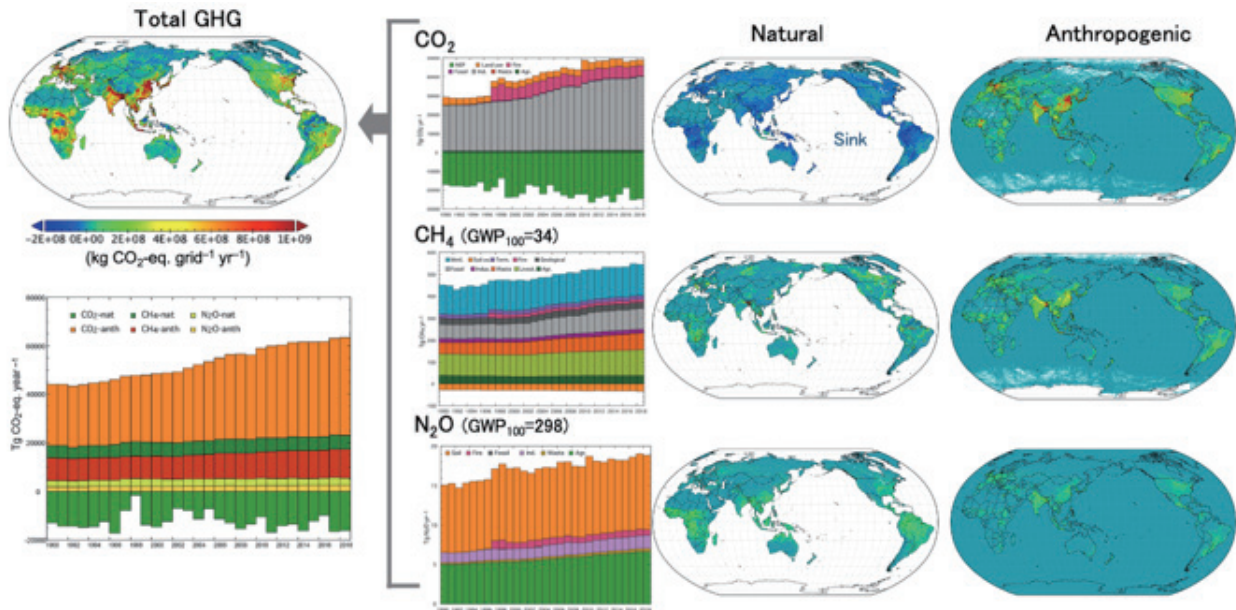
Figure 10. Global GHG budgets estimated by the bottom-up approach. Maps show mean annual budgets during 2000–2018.

Regional GHG budget

We present a regional GHG budget for East Asia. In this region, natural and anthropogenic CO_2 budgets over 2010 to 2018 were estimated as -1639 ± 446 (net sink) and $12,500 \pm 500$ Tg CO_2 yr^{-1} (source), respectively (Fig. 11). The regional total CO_2 budget was a net source of $10,800 \pm 300$ Tg CO_2 yr^{-1}. Natural and anthropogenic CH_4 emissions over 2010 to 2018 were estimated as 10.5 ± 0.9 and 69.1 ± 1.3 Tg CH_4 yr^{-1}, respectively. The high contribution of anthropogenic emissions (87% of total budget), especially from fossil fuel mining, characterizes the CH_4 budget of this region. Using the GWP over 100 years, the annual mean CH_4 source was equivalent to 2707 ± 53 Tg CO_2-eq yr^{-1}. Natural and anthropogenic N_2O emissions over 2010 to 2018 were estimated as 0.86 ± 0.08 and 0.71 ± 0.01 Tg N_2O yr^{-1}, respectively. Using the GWP over 100 years, the annual mean N_2O source was equivalent to 571.5 ± 25.1 Tg CO_2-eq yr^{-1}.
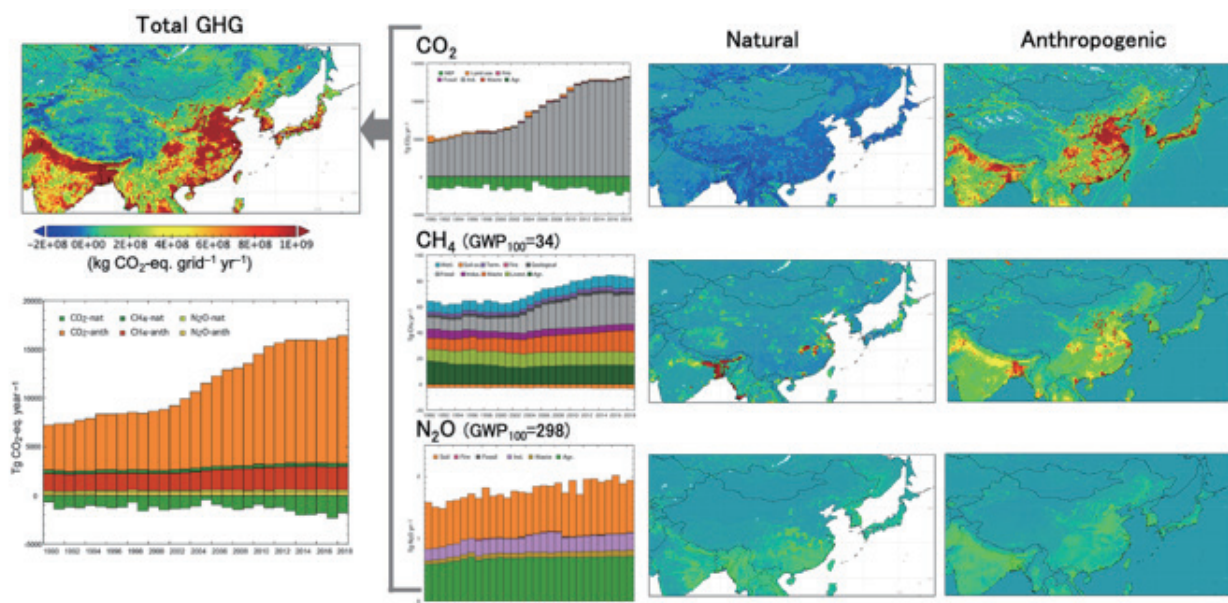
Figure 11. GHG budgets of East Asia estimated by the bottom-up approach. Maps show mean annual budget during 2000–2018.

National GHG budget

We obtained national GHG budgets for almost all countries by the bottom-up approach and present here the budget for Japan. In this country, natural and anthropogenic CO_2 budgets over 2010 to 2018 were estimated as -106 ± 53 (net sink) and 970 ± 38 Tg CO_2 yr^{-1} (source), respectively (Fig. 12). In the national annual CO_2 budget, Japan was a net source of 861 ± 66 Tg CO_2 yr^{-1}. Ecosystem CO_2 uptake (mainly by forests) offset approximately 11% of the emissions from human activities in Japan. Natural and anthropogenic CH_4 emissions over 2010 to 2018 were estimated as 0.66 ± 0.01 and 1.9 ± 0.09 Tg CH_4 yr^{-1}, respectively. The high contribution of anthropogenic emissions (75% of the total), especially from livestock and agricultural soils, characterizes the CH_4 budget of this country. Using the GWP over 100 years, annual mean CH_4 emissions were equivalent to 88.6 ± 3.0 Tg CO_2-eq yr^{-1}. Regional natural and anthropogenic N_2O emissions over 2010 to 2018 were estimated as 0.041 ± 0.001 and 0.028 ± 0.001 Tg N_2O yr^{-1}, respectively. Using the GWP over 100 years, the annual mean N_2O source was equivalent to 30.0 ± 0.7 Tg CO_2-eq yr^{-1}.
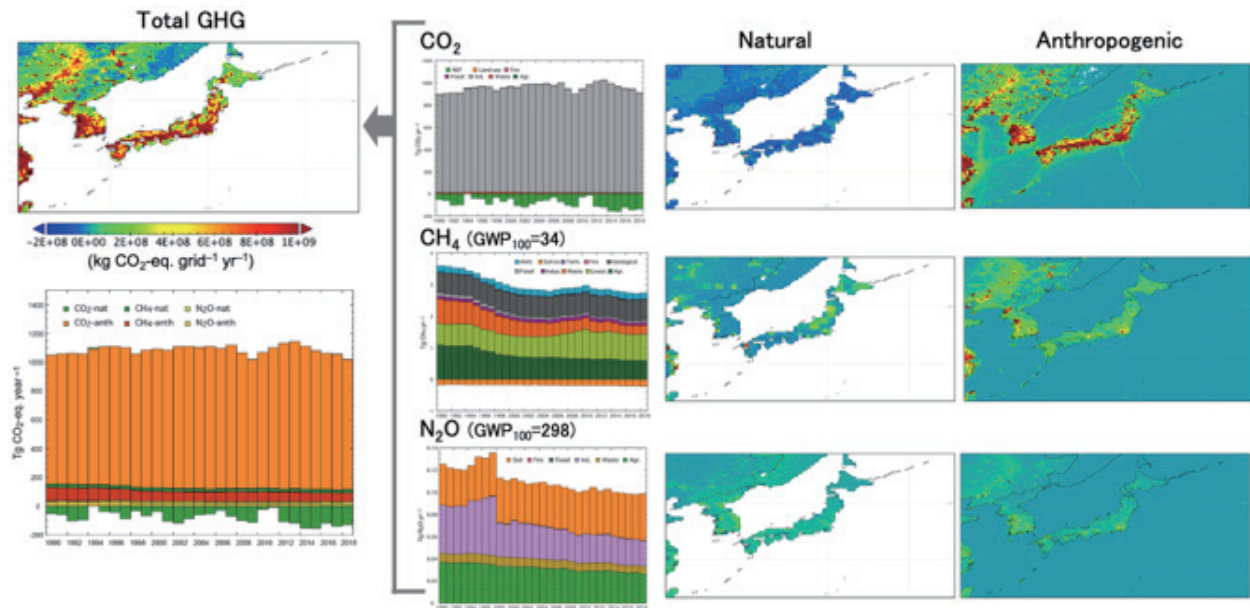
Figure 12. GHG budgets of Japan estimated by the bottom-up approach. Maps show mean annual budget during 2000–2018.

3.3. Comparison between top-down and bottom-up estimates

The difference between the top-down and bottom-up approaches indicates the range of uncertainties associated with assumptions and methods. Tables 1 and 2 compare the global and regional (East Asia) GHG budgets estimated by the top-down and bottom-up approaches for 5-year periods from 1996 to 2020. The two approaches used different data and models, leading to the different directions and magnitudes of biases and errors. Previous studies comparing the top-down and bottom-up results imply that fundamental, conceptual (or terminological) differences between the two approaches could exert substantial influences. For example, there remains ambiguity in the definition of 'natural' and 'anthropogenic' emissions, such that land-use and biomass burning emissions could occur heterogeneously in space and time and by various reasons. Also, it is still difficult to include lateral flows such as riverine export and transport of agricultural products and harvested wood in both top-down and bottom-up approaches. These issues are contemporary topics for the carbon cycle and greenhouse gas research communities.

In this report, to avoid conceptual ambiguity and to ensure accuracy in the comparison between results of the two approaches, we adopted the following definitions. For CO_2, fossil fuel combustion emissions comprise anthropogenic emissions, and net ecosystem production and land-use emissions comprise net natural emissions (including sinks). These definitions avoid the difficulty and uncertainty associated with specification of land-use emissions from forest and grassland areas. For CH_4 and N_2O, total global and regional budgets including both natural and anthropogenic emissions are compared, because these gases have a wide variety of emission sources, which are difficult to distinguish by using atmospheric information. Despite the simplifications, the comparison presented here is still useful to examine the consistency of our GHG budgets, especially in terms of applicability to the GST.

Table 1. Comparison of global land total GHG budgets between top-down and bottom-up approaches (mean ± SD of interannual variability).

			1996–2000	2001–2005	2006–2010	2011–2015	2016–2020
CO_2	Nat. + LUC	top-down (NISMON)	−1.39 ± 0.87	−1.46 ± 0.95	−2.90 ± 0.61	−2.51 ± 1.40	−1.86 ± 0.71
		(MIROC4-ACTM)	--	−1.67 ± 0.63	−2.89 ± 0.46	−3.04 ± 0.80	−2.73 ± 0.67
		bottom-up	−3.01 ± 1.72	−2.48 ± 0.68	−3.45 ± 0.52	−3.95 ± 0.52	−3.84 ± 0.74
	Anthr. (FF)	top-down & bottom-up	6.68 ± 0.11	7.48 ± 0.42	8.68± 0.24	9.59 ± 0.11	9.78 ± 0.20
CH_4	Total	top-down (MIROC4-ACTM)	548.5 ± 14.8	560.4 ± 18.0	563.7 ± 8.2	579.1 ± 12.9	599.4 ± 10.0
		bottom-up	440.1 ± 7.5	451.0 ± 7.2	476.7 ± 6.2	496.7 ± 5.3	515.0 ± 9.1
N_2O	Total	top-down (MIROC4-ACTM)	15.6 ± 0.7	15.6 ± 0.3	16.4 ± 1.0	17.0 ± 0.7	17.5 ± 0.7
		bottom-up	17.0 ± 0.7	17.0 ± 0.3	17.9 ± 0.5	18.2 ± 0.1	19.0 ± 0.3

CO_2 in Pg C yr^{-1}, CH_4 in Tg CH_4 yr^{-1}, N_2O in Tg N_2O yr^{-1}

Table 2. Comparison of land total GHG budgets between top-down and bottom-up approaches for East Asia (mean ± SD of interannual variability).

			1996–2000	2001–2005	2006–2010	2011–2015	2016–2020
CO_2	Nat. + LUC	top-down	−0.20 ± 0.43	−0.02 ± 0.28	−0.19 ± 0.41	−0.05 ± 0.31	0.28 ± 0.14
		bottom-up	−0.32 ± 0.09	−0.31 ± 0.11	−0.31 ± 0.06	−0.43 ± 0.10	−0.53 ± 0.08
	Anthr. (FF)	bottom-up	1.47 ± 0.03	1.83 ± 0.25	2.63 ± 0.20	3.29 ± 0.05	3.34 ± 0.06
CH_4	Total	top-down (MIROC4-ACTM)	--	52.2 ± 1.7	57.7 ± 2.1	60.1 ± 2.5	48.9 ± 2.4
		bottom-up	61.3 ± 1.1	64.2 ± 3.3	73.5 ± 2.3	79.7 ± 1.6	80.7 ± 1.0
N_2O	Total	top-down (MIROC4-ACTM)	1.48 ± 0.13	1.57 ± 0.10	1.76 ± 0.13	1.71 ± 0.12	1.75 ± 0.16
		bottom-up	1.72 ± 0.06	1.75 ± 0.07	1.85 ± 0.07	1.90 ± 0.10	2.02 ± 0.11

CO_2 in Pg C yr^{-1}, CH_4 in Tg CH_4 yr^{-1}, N_2O in Tg N_2O yr^{-1}

4. Concluding remarks

This report demonstrated the global, regional, and national GHG budgets created using observational data and models for the purpose of providing evidence to the GST of the Paris Agreement based on the best available science. The GHG monitoring system proposed by the SII-8 project adequately captured spatial and temporal properties of the GHG budgets, allowing us to detect mitigation efforts and leakages in an objective and transparent manner. The system well covers the Asia-Pacific region, complimenting activities in other regions such as the Copernicus and Integrated Carbon Observation System in Europe and the North American Carbon Program. Note that the present GHG budget estimations were accomplished by using our own observational and model simulation data, in conjunction with open datasets (e.g., emission inventories and satellite products). Through collaborative works from monitoring to modeling, the project enables us to quickly report to stakeholders (Fig. 13). There remain, nevertheless, substantial uncertainties due to sparse observational coverage, errors in immature models, and biased emission inventories. Fortunately, ongoing efforts in the project are expected to overcome these limitations and provide more reliable GHG budgets in support of transparent accomplishment of the GST.
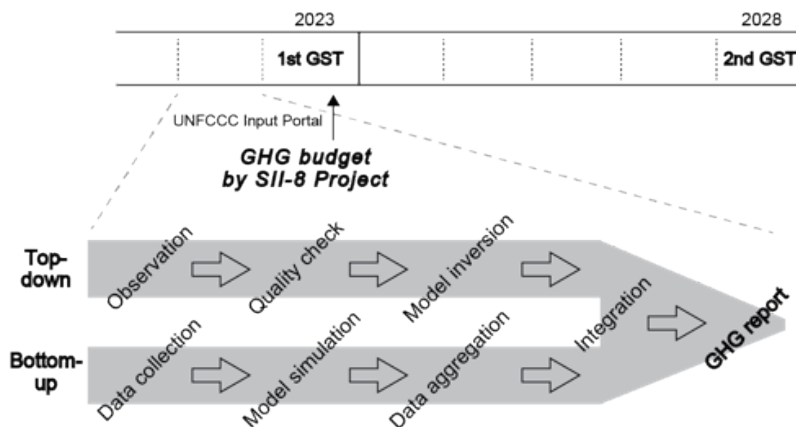
Figure 13. Expected timeline of the contribution of GHG budgets to the Global Stocktake (GST).

Corresponding GST1 Guiding Questions (by SB chairs, ver. 20 Oct. 2021) and our answers

\<Mitigation\>

Q2. *What is the collective progress made towards achieving the long-term mitigation goal in Article 4.1 of the Paris Agreement, in the light of equity and the best available science?*

A2. This report provides our up-to-date estimates of global, regional, and national greenhouse gas (GHG) budgets mainly based on atmospheric observations and modeling, allowing us to transparently examine the state of emission reduction toward achieving the long-term mitigation goal.

Q3. *What are the projected global GHG emissions and what actions are Parties undertaking to achieve a balance between anthropogenic emissions by sources and removals by sinks of GHGs, on the basis of equity, and in the context of sustainable development and efforts to eradicate poverty (Article 4.1 Paris Agreement, Decision 19/CMA.1, paragraph 36(b))?*

A3. The GHG budgets provided in this report account for not only net budgets but also sources and sinks of natural and anthropogenic sectors, allowing us to examine the balance between anthropogenic GHG emissions by sources and removals by sinks. By using the Earth system model, our project is also examining the projected global GHG emissions in terms of mitigation effectiveness.

\<Cross-cutting\>

Q16. *To achieve the purpose and long-term goals of the Paris Agreement (mitigation, adaptation, and finance flows and means of implementation, as well as loss and damage, response measures), in the light of equity and the best available science, taking into account the contextual matters in the preambular paragraphs of the Paris Agreement:*
a. What are the good practices, barriers and challenges for enhanced action?
b. What is needed to make finance flows consistent with a pathway towards low GHG emissions and climate-resilient development?
c. What are the needs of developing countries related to the ambitious implementation of the Paris Agreement?

A16-c. The methodology of GHG monitoring adopted in this report is applicable to developing countries and therefore supports their ambitious implementations of the Paris Agreement, at least in terms of mitigation.

Q17. *What is needed to enhance national level action and support, as well as to enhance international cooperation for climate action, including in the short term?*

A17. Reliable GHG budgets are prerequisites for national and international actions; therefore, establishing a continuous GHG monitoring system that encompasses multi-scale observations and modeling through international collaborations is needed.

Q18. *What is the collective progress made by non-Party stakeholders, including indigenous peoples and local communities, to achieve the purpose and long-term goals of the Paris Agreement, and what are the impacts, good practices, potential opportunities, barriers and challenges (Decision 19/CMA.1, paras 36(g) and 37(i))?*

A18. This report comprehensively covers GHG budgets and therefore is useful for non-Party stakeholders to obtain overviews for planning actions toward long-term goals.

Data availability

• CONTRAIL-CME

CO_2: https://www.nies.go.jp/doi/10.17595/20210827.001-e.html

• Hateruma Station observation data

CO_2: http://www.nies.go.jp/doi/10.17595/20160901.001-e.html

CH_4: http://www.nies.go.jp/doi/10.17595/20160901.003-e.html

• MIROC4-ACTM data:

CO_2: https://doi.org/10.5281/zenodo.5776197, https://doi.org/10.5281/zenodo.5776212

CH_4: https://doi.org/10.5281/zenodo.5920070

N_2O: https://doi.org/10.5281/zenodo.5889524

• NISMON-CO_2:

CO_2: https://www.nies.go.jp/doi/10.17595/20201127.001-e.html

• VISIT data:

CO_2, CH_4, N_2O: https://www.nies.go.jp/doi/10.17595/20210521.001-e.html

References

Akagi SK, Yokelson RJ, Wiedinmyer C, et al. (2011) Emission factors for open and domestic biomass burning for use in atmospheric models. Atm Chem Phys 11: 4039–4072. DOI: 10.5194/acp-11-4039-2011

Bisht JSH, Machida T, Chandra N, et al. (2021) Seasonal variations of SF_6, CO_2, CH_4, and N_2O in the UT/LS region due to emissions, transport, and chemistry. J Geophys Res Atm 126: e2020JD033541. DOI: 10.1029/2020JD033541

Chandra N, Patra PK, Bisht JS, et al. (2021a) Emissions form the oil and gas sectors, coal mining and ruminant farming drive methane growth over the past three decades. J Meteor Soc Jpn 99: 309–337. DOI: 10.2151/jmsj.2021-015

Chandra N et al. (2021b) Estimated regional CO_2 flux and uncertainty based on an ensemble of atmospheric CO_2 inversions. Atmos Chem Phys Discuss, in review, DOI: 10.5194/acp-2021-1039

Crippa M, Solazzo E, Huang G, et al. (2020) High resolution temporal profiles in the emissions database for global atmospheric research. Scientific Data 7: 121. DOI: 10.1038/s41597-020-0462-2

Friedlingstein P, Jones MW, O'Sullivan M, et al. (2021) Global carbon budget 2021. Earth System Sci Data Discuss DOI: 10.5194/essd-2021-386

Hajima T, Watanabe M, Yamamoto A, et al. (2020) Development of the MIROC-ES2L Earth system model and the evaluation of biogeochemical processes and feedbacks. Geosci Model Dev 13: 2197–2244. DOI: 10.5194/gmd-13-2197-2020

Iida Y, et al. (2021), Global trends of ocean CO_2 sink and ocean acidification: an observation-based reconstruction of surface ocean inorganic carbon variables. J Oceanogr 77, 323–358. DOI:10.1007/s10872-020-00571-5

Inatomi, M., A. Ito, K. Ishijima, S. Murayama (2010) Greenhouse gas budget of a cool temperate deciduous broadleaved forest in Japan estimated using a process-based model. Ecosystems 13, 472–483, DOI: 10.1007/s10021-010-9332-7

Ishii M, Kosugi N, et al. (2011), Ocean acidification off the southcoast of Japan: A result from time series observations of CO_2 parameters from 1994 to 2008, J Geophys Res, 116, C06022, DOI:10.1029/2010JC006831

Ito A (2019) Disequilibrium of terrestrial ecosystem CO_2 budget caused by disturbance-induced emissions and non-CO_2 carbon export flows: a global model assessment. Earth System Dyn 10, 685–709. DOI: 10.5194/esd-10-685-2019

Ito A, Inatomi M (2012) Use of a process-based model for assessing the methane budgets of global terrestrial ecosystems and evaluation of uncertainty. Biogeosci 9, 759–773. DOI: 10.5194/bg-9-759-2012

Ito A, Nishina K, Ishijima K, et al. (2018) Emissions of nitrous oxide (N_2O) from soil surfaces and their historical changes in East Asia: a model-based assessment. Progr Earth Planet Sci 5. DOI: 10.1186/s40645-018-0215-4

Jones MW, Andrew RM, Peters GP, et al. (2021) Gridded fossil CO_2 emissions and related CO_2 combustion consistent with national inventories 1959–2018. Scientific Data 8: 2. DOI: 10.1038/s41597-020-00779-6

Kobayashi S, Ota Y, Harada H, et al. (2015) The JRA-55 reanalysis: General specification and basic characteristics. J Meteor Soc Jpn 93: 5–48. DOI: 10.2151/jmsj.2015-001

Machida T, Matsueda H, Sawa Y, et al. (2008) Worldwide measurements of atmospheric CO_2 and other trace gas species using commercial airlines. J Atm Ocean Technol 25: 1744-1754. DOI: 10.1175/2008JTECHA1082.1

Terao Y, Mukai H, Nojiri Y, et al. (2011) Interannual variability and trends in atmospheric methane over the western Pacific from 1994 to 2010. J Geophys Res 116: DOI:10.1029/2010JD15467

Tohjima Y, Machida T, Utiyama M, et al. (2002) Analysis and presentation of in situ atmospheric methane measurements from Cape Ochi-ishi and Hateruma Island. J Geophys Res 107, 4148. DOI: 10.1029/2001JD001003

Tohjima Y, Minejima C, Mukai H, et al. (2012) Analysis of seasonality and annual mean distribution of atmospheric potential oxygen (APO) in the pacific region. Global Biogeochem Cycles 26: 10.1029/2011GB004110. DOI: 10.1029/2011GB004110

Tohjima Y, Kubo M, Minejima C, et al. (2014) Temporal changes in the emissions of CH_4 and CO from China estimated from CH_4 / CO_2 and CO / CO_2 correlations observed at Hateruma Island. Atm Chem Phys 14: 1663–1677. DOI: 10.5194/acp-14-1663-2014

Tohjima Y, Patra PK, Niwa Y, et al. (2020) Detection of fossil-fuel CO_2 plummet in China due to COVID-19 by observation at Hateruma. Sci Rep 10: 18688. DOI: 10.1038/s41598-020-75763-6

Tsuboi K, et al. (2013), Evaluation of a new JMA aircraft flask sampling system and laboratory trace gas analysis system. Atm Measur Tech, 6, 1257–1270, DOI: 10.5194/amt-6-1257-2013

Tsuboi K, et al. (2017), Inter Comparison Experiments for Greenhouse Gases Observation　(iceGGO) in 2012–2016, Tech Rep Meteorol Res Inst. No.79. DOI:10.11483/mritechrepo.79

Tsutsumi Y, Mori K, Ikegami M, et al. (2006) Long-term trends of greenhouse gases in regional and background events observed during 1998–2004 at Yonagunijima located to the east of the Asian continent. Atm Env 40: 5868–5879. DOI: 10.1016/j.atmosenv.2006.04.036

Umezawa T, Matsueda H, Oda T, et al. (2020) Statistical characterization of urban CO_2 emission signals observed by commercial airline measurements. Sci Rep 10: 7963. DOI: 10.1038/s41598-020-64769-9

van der Werf GR, Randerson JT, Giglio L, et al. (2017) Global fire emissions estimates during 1997–2016. Earth Sys Sci Data 9: 697–720. DOI: 10.5194/essd-9-697-2017

Watanabe F, Uchino O, Joo Y, et al. (2000) Interannual variation of growth rate of atmospheric carbon dioxide concentration observed at the JMA's three monitoring stations: Large increase in concentration of atmospheric carbon dioxide in 1998. J Meteorol Soc Jpn 78: 673–682. DOI:10.2151/jmsj1965.78.5_673

Wolter, K., and M. S. Timlin (2011), El Niño / Southern Oscilaltion behaviour since 1871 as diagnosed in an extended multivariate ENSO index (MEI.ext). Int J Climatol 31: 1074–1087. DOI: 10.1002/joc.2336

Yokota T, Yoshida Y, Eguchi N, et al. (2009) Global Concentrations of CO_2 and CH_4 retrieved from GOSAT: First Preliminary Results. SOLA 5: 160–163. DOI:10.2151/sola.2009-041

Yoshida Y, Kikuchi N, Morino I, et al. (2013) Improvement of the retrieval algorithm for GOSAT SWIR XCO_2 and XCH_4 and their validation using TCCON data. Atm Measur Tech 6: 1533–1547. DOI: 10.5194/amt-6-1533-2013

Contacts

International Coordination Office, National Institute for Environmental Studies, Japan

Notes:

ppm: parts per million abbreviating dry air mole fraction of 10^{-6} mol mol^{-1}

Pg: petagram (10^{15} g)

Tg: teragram (10^{12} g)

GWP: Global Warming Potential